Doppler Free Saturation Spectroscopy of Rubidium

Alin Airinei*
Department of Physics, Stony Brook University, Stony Brook, NY 11794
(Dated: February 2020)

To analyze the hyperfine splitting of the $5^2p_{\frac{3}{2}}$ state of ^{87}Rb the technique of *Doppler-Free Saturation Spectroscopy* was employed to induce the depletion of the ground state and counter the broadening effects caused by frequency shifts due to thermal motion within the sample. We test the accuracy of our method by measuring the frequency separation between the allowed levels and compare our results with the accepted values.

I. Introduction

Rubidium(Rb) is part of the alkali metals and has atomic number 37. Alkali elements are characterized by a closed shell configuration of the inner electrons and a single valence electron which gives them a "*hydrogen-like*" structure and properties.

The electron configuration of rubidium is $1s^22s^22p^63s^23p^63d^{10}4s^24p^65s$ with the 36 inner electrons paired and the outer one in the 5s orbital. Therefore it is convenient to neglect the paired electrons and treat rubidium as a single electron hydrogen atom[1].

The two naturally occurring isotopes of rubidium are the stable ^{85}Rb, with a natural abundance of 72.2%, and the unstable ^{87}Rb, with a natural abundance of 27.8%. The decay rate of ^{87}Rb is extremely slow, which makes it virtually stable for any practical purpose. This experiment will focus on ^{87}Rb[2].

II. Theory

II.1. Fine Structure

The parameters describing the outer electron are the orbital angular momentum **L** and the electron angular momentum **S**, which combine according to the rules of vector addition to give the total non-nuclear angular momentum **J**.

$$\mathbf{J} = \mathbf{L} + \mathbf{S} \tag{1}$$

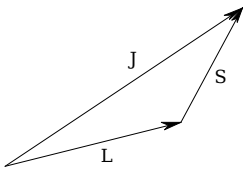

Figure 1. Coupling of orbital angular momentum (L) and spin angular momentum (S), with the total angular momentum (L) obtained by vector addition.

* alin.airinei@stonybrook.edu
zachary.kluger@stonybrook.edu

Each of the angular momenta discussed above has an associated dipole momentum $\mu_{\mathbf{S}}$ and $\mu_{\mathbf{L}}$ coupled magnetically and which, according to orientation will lead to different interaction energies[1].

In the ground state **L**=0, and $\mathbf{S} = \frac{1}{2}$. This will yield the single valued total momentum $\mathbf{J} = \frac{1}{2}$. Therefore, in "$(nl)^{2S+1}L_J$" notation, the ground electronic state is $(5s)^2S_{1/2}$, i.e. n=5, l=0, $S = \frac{1}{2}$, L = 0, and $J = \frac{1}{2}$[3].

For the first excited state (P), **J** will have only the values $|L + S|$ and $|L - S|$, which give two fine structure levels, $(5p)^2P_{\frac{1}{2}}$, and $(5p)^2P_{\frac{3}{2}}$ [1]. The dependence of the fine splitting on **J** will also cause the transition line (D) between L = 0 and L = 1 to be split into two components, the D_1 line connecting levels $(5s)^2S_{\frac{1}{2}}$ and $(5p)^2P_{\frac{1}{2}}$, and the D_2 line connecting levels $(5s)^2S_{\frac{1}{2}}$ and $(5p)^2P_{\frac{3}{2}}$[2].

II.2. Hyperfine Structure

When taking into account the nuclear angular momentum **I** the total angular momentum of the atom becomes:

$$\mathbf{F} = \mathbf{J} + \mathbf{I} \tag{2}$$

Analogous to the case of the total electron angular momentum, the atomic momentum will take only the values of $|J - I|$ and $|J + I|$, and thus will cause a further splitting of the energy levels called *hyperfine splittings* [2].

The diode laser used for the current experiment can only be tuned at around 780nm, therefore, our study will focus on the D_2 line [3]. Based on the above, for the D_2 line **F** can take any of the values 1 and 2, for the ground state and 0, 1, 2, 3 for the excited state as shown in Fig. 2 [2].

For our current purpose we do not consider hyperfine splittings due to the Zeeman effect, and ignoring the weak effects from the Earth's magnetic field we consider the external magnetic field $H_0 = 0$. Thus, the splitting of the energy levels for particular values of **I** and **J** can formally be characterized by a Hamiltonian as [2, 3]:

$$\mathcal{H} = [A\mathbf{I}\cdot\mathbf{J}] + \left[B\frac{3(\mathbf{I}\cdot\mathbf{J})^2 + \frac{3}{2}\mathbf{I}\cdot\mathbf{J} - \mathbf{I}(\mathbf{I}+1)\mathbf{J}(\mathbf{J}+1)}{2\mathbf{I}(2\mathbf{I}-1)\mathbf{J}(2\mathbf{J}-1)}\right]$$

The second term in square brackets is the electric quadrupole interaction which vanishes unless $\mathbf{I} \geq 1$, and

$\mathbf{J} \geq 1$. Therefore, for the ground state, the Hamiltonian would have only the first term, while for the excited state both terms would apply[3].

For $\mathbf{J} = \frac{1}{2}$ (the ground state of ^{87}Rb) the Hamiltonian splits with the magnetic dipole hyperfine interaction $\mathbf{F} = \mathbf{I} \pm \frac{1}{2}$ giving the $\mathbf{F} = 1$ and $\mathbf{F} = 2$ levels with an energy separation given by[3]:

$$\begin{aligned}\Delta E &= A_{87}(\mathbf{I} + \frac{1}{2}) \\ &= 2A_{87}\end{aligned}$$

For the excited state with $\mathbf{I} = \frac{3}{2}$ and $\mathbf{J} = \frac{3}{2}$ (for ^{87}Rb), the energy separation will be determined by both the magnetic dipole and electric quadrupole terms while $\mathbf{F}$ will acquire two extra values for a total set of: $\mathbf{F} = 0, 1, 2, 3$ [3, 4]:

$$\Delta E = A_{87}\mathbf{F} + B_{87}\frac{\frac{3}{2}\mathbf{F}[\mathbf{F}^2 - \mathbf{I}(\mathbf{I}+1) - \mathbf{J}(\mathbf{J}+1) + \frac{1}{2}]}{\mathbf{I}(2\mathbf{I}-1)\mathbf{J}(2\mathbf{J}-1)}$$

To obtain the energy separation in terms of frequency we divide ΔE by Planck's constant $\hbar$. The values listed in Fig. 2 are taken from precise measurements of the hyperfine structure as reported in [2]. Our purpose is to verify and test our own results against the listed values.

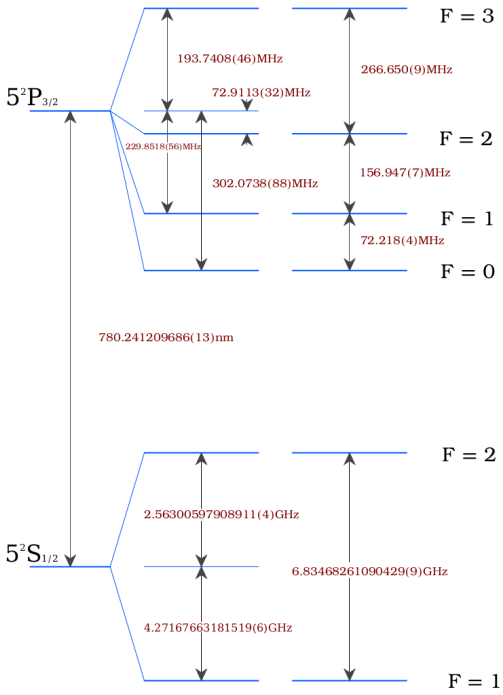

Figure 2. Hyperfine structure of the ^{87}Rb ground and first excited levels. The diagram concept was borrowed from [2] with the original values published in [5, 10].

III. Experimental Setup

III.1. Optical Bench Setup

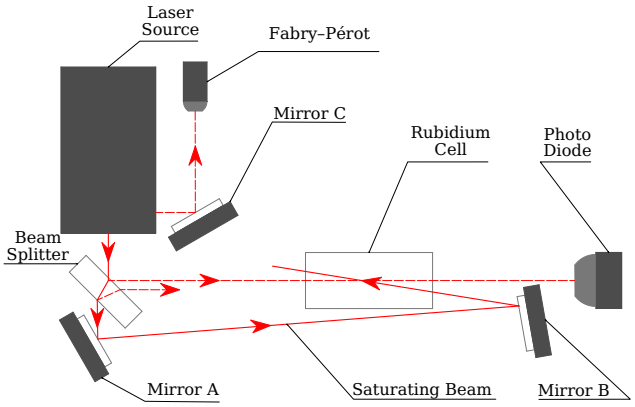

Figure 3. The optical bench setup.

The diagram in Fig. 3 illustrates schematically the optical circuit used to perform our measurements.

Light from the laser source reaches a beam splitter where it is partially transmitted and partially reflected. The reflected beam will travel across the rubidium vapor cell and reach the photo diode. This portion of the circuit will produce the Doppler broadened absorption spectra.

The transmitted beam will reach mirror A where it will further be reflected to mirror B and back toward the rubidium cell where it will intersect the first beam. This is the "optical pump" of the circuit which has the purpose of countering the Doppler broadening effects of the first beam by saturating the absorption spectra. The following section will briefly describe the theoretical background of the two processes.

A third part of the optical circuit includes a second beam produced by the laser assembly which is further reflected by mirror C toward the Fabry-Pérot resonator. This part will be explained in the measuring and control section bellow.

We have to also mention that the initial beam splitter will produce a second weak reflection in the direction of the photo diode due to it's thickness. In a setup with two photo diodes the first beam that meets the saturation beam is called the "overlap beam" and the second is called the "reference beam"[6]. We only use one of the probe beams for the current experiment and we initially encountered some calibration issues that might have been due to the second reflection which we eventually overcame by careful alignment of the mirrors. Another option would be to place a stopper in its path or to deflect it elsewhere.

III.2. Doppler Broadening and Optical Pumping

If the saturation beam from mirror A is blocked before reaching the vapor cell the signal from the photo diode displayed on the oscilloscope will be Doppler broadened. The effect is due to the thermal motion of the atoms in the cell which causes most atoms to receive the light Doppler shifted from the laser frequency[6].

To counter the Doppler broadening effect we use the technique of laser-saturated absorption spectroscopy by using a stronger counter-propagating beam (the pump beam) to reduce the absorption rate of the weaker probe beam. The result of this procedure is the appearance of dips in the the Doppler broadened line which correspond to atomic transitions from the ground state to the hyperfine levels of the excited state[6].

Another type of transition dips that occur are crossover transitions. A crossover happens when the laser frequency is tuned such that atoms with velocity $-V_{z1}$ see the pump beam red shifted to the resonant frequency ν_1 and the probe beam blue shifted to $\nu 2$[6]. the Doppler shift for each case is given by:

$$\nu_1 = \nu_c(1 - \frac{V_{z1}}{c})$$

$$\nu_2 = \nu_c(1 + \frac{V_{z1}}{c})$$

Solving the above system for the crossover frequency yields:

$$\nu_c = \frac{\nu_1 + \nu_2}{2} \tag{3}$$

We presently employ Eqn. (3) in our analysis to identify the crossover transitions.

III.3. Measuring and Control Equipment

The control section of our setup includes a Fabry-Pérot spectrum scan controller. Fig. 4 shows schematically the path of the laser beam as it leaves the source assembly. Part of the light is reflected by a prism splitter toward the side of the case and then directed toward the Fabry-Pérot interferometer.

To scan the laser beam entering the interferometer the controller varies the displacement of the mirrors by means of tuning the ramp voltage applied to piezoelectric actuators. By making the spacing equal to an integral number of half-wavelengths of the incoming laser beam, constructive interference will occur[7].

The next three elements of the control rack include a laser diode current controller, a temperature controller, and a modulator. The current controller and the temperature controller are the core driving elements behind the laser diode which assure the stability of it's operation[8].

In this experiment we use a modulator to trigger the current controller with the purpose of providing a periodic sweep through a range of wavelengths centered around 780nm which will ensure the probe and saturation beams will interact with different parts of the thermal velocity distribution[6].

For measuring purposes we use two oscilloscopes, one measuring the Fabry-Pérot scanner and the second connected to the probe photo diode.

To calibrate our sweep we use the dual channel capability of the first oscilloscope to fit two resonance peaks from the Fabry-Pérot interferometer on one side of the trigger's ramp signal. By knowing the free spectral range to be 10GHz we use the distance between the resonance peaks as measured on the oscilloscope (in time units) to convert our time base into a frequency base which we then transfer to the scale of the second oscilloscope which measures the signal from the photo diode.

For the last part of the experiment, when we look at individual peaks we perform another scale conversion, but this time, we use the full-width half-maximum of the measured peak as our étalon.

To complete the discussion of our methodology we have to mention that when scanning individual peaks we are taking measurements of both Doppler broadened and saturated signals and subtract them to isolate the hyperfine features by removing the Doppler background .

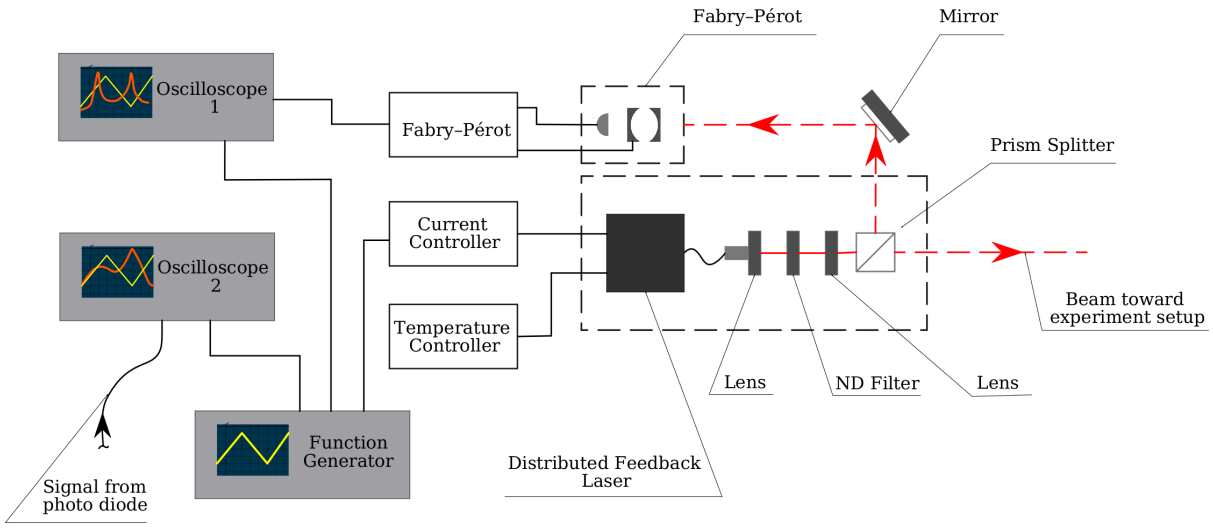

Figure 4. The Measuring and control rack includes the Fabry-Pérot controller, the laser current and temperature controllers, a function generator and two oscillators.

IV. Results

IV.1. Doppler-broadened Fine Structure

The Doppler-broadened spectrum of the ground state for our Rb test sample is shown in Fig. 5. As our sample is a mixture of two isotopes with different nuclear magnetic dipole moments we obtain four transition peaks as expected (two for each isotope).

The peaks were fit using Gaussian models and the observed difference in amplitude between ^{85}Rb and ^{87}Rb spectra occurs due to the natural abundance of each isotope.

The frequency separation between ^{87}Rb F=1 and F=2 levels was thus measured at $6.355 \pm 0.003GHz$ which is $\approx$ 93% of the expected value by comparison with our reference values (Fig. 2).

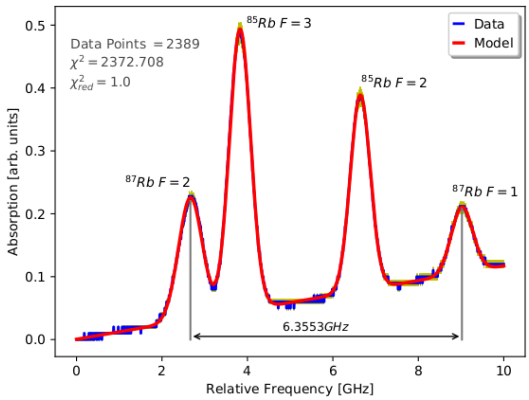

Figure 5. The Gaussian fit to the Doppler broadened signal showing the frequency separation between the ^{87}Rb F=1 and F=2 levels.

To zoom in on the $5^2s_{\frac{1}{2}} \longrightarrow 5^2p_{\frac{3}{2}}$ transition we tweaked the laser frequency by changing the ramp amplitude and offset on the modulator to scan only the ^{87}Rb F=1 transition.

IV.2. Doppler-free Characteristics

After completing the magnification procedure we took measurements of both the Doppler-broadened signal, and, by unblocking the pump, of the Doppler-free signal. We performed a Gaussian fit on the broad signal in order to equate the FWHM with the previous value (measured before magnification) and thus realized our final scale conversion. The two signals are shown superimposed in Fig. 6 with the "pumped" signal (purple) presenting lamb dips.

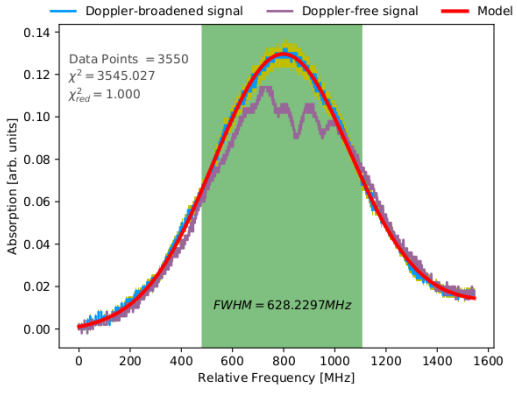

Figure 6. The graph shows the magnified ^{87}Rb Doppler-broadened signal with the shaded region showing the FWHM after the final scale conversion. Also, for comparison, the lamb dips produced by un-blocking the pump beam are also illustrated.

IV.3. Hyperfine Splitting

As a last step the Doppler background was subtracted from the "pumped" signal to obtain a final Doppler-free profile of the hyperfine splitting of the transition.

The result was particularly noisy, and the prime candidate for this lack of resolution is the less than ideal tuning of our laser beam intensities (probe, pump, and reference).

As properly explained in different sources (e.g. in reference [9]), measuring and adequately selecting the beam intensities can be critical, with the probe and reference beam required to be at less than 1% of the saturating beam intensity which in turn should be tuned according to the lifetime of the excited state of Rb ($\approx 28ns$) at $\approx 1.6mW/cm^2$. This intensity difference can be achieved by the use of ND filters in the path of the probe and/or reference beams.

In addition to the above we also used only one photodiode for both probe and reference beams which complicates things even further. In the end, together with digitization and other possible unaccounted effects (such as a possible increase in thermal noise, resonances resulted from the initial offset of the signals before subtraction) we were left with a noise to signal ratio that made most features hardly distinguishable.

Considering the above we were still able to distinguish three most prominent features which we identified as roughly corresponding to the F=0, F=1, and F=2 hyperfine levels. We used the Moffat model to fit individual peaks. The Moffat model produced smaller offsets than the Lorentzian models which are customarily used and reported in the Rubidium spectroscopy literature. The results are summarized in Fig. 7. The model was plotted against the original data to show both the correspondence with the measurements and to show by comparison the obscuring effects of the background noise.

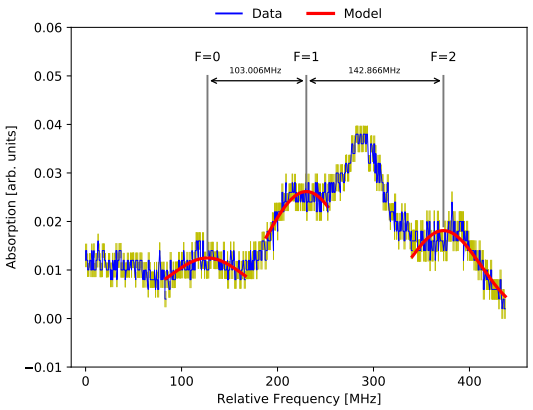

Figure 7. Hyperfine features of the $5^2s_{\frac{1}{2}}$ F=1 transition to $5^2p_{\frac{3}{2}}$ F'=0, 1, 2. Moffat models were used to fit individual peaks. (The error bars are color-coded yellow).

Due to the stated lack of resolution the cross-over frequencies were not distinguishable at all, and we are left with the only qualitative conclusion that the highest (central) amplitude in the signal is a mixture of the C_{02} and C_{12}, with the indices indicating the parent transitions.

The final results of our measurements are listed in the table below. We obtained a 91% of the expected value for the F=1 to F=2 energy gap, and only a rough 57% agreement for the separation of the F=0 and F=1 levels. Experimental errors throughout our analysis were estimated based on instrumentation accuracy, and all our fit models yielded reduced χ^2 values close to 1.

Hyperfine Splitting	Measured [MHz]	Reference[MHz]
$F_0 \longleftrightarrow F_1$	103.006 ± 1.703	72.218(4)
$F_1 \longleftrightarrow F_2$	142.866 ± 1.48	156.947(7)

Table I. Frequency separation of the hyperfine splitting levels compared with the reference values.

V. Conclusions

We first produced a Doppler-broadened fine structure spectrum of our isotope mixture of ^{85}Rb and ^{87}Rb, with two sets of hyperfine transitions, adding to a total of four absorption peaks for the ground level of our test sample.

By using a counter-propagating saturating beam to induce the depletion of the ground state we revealed the hyperfine features in the form of lamb dips.

To increase the resolution we further calibrated the laser to scan the transition of the F=1 level of the ground state to the $5^2p_{\frac{3}{2}}$ state.

Once the magnification was achieved we subtracted the Doppler background from the saturated signal to obtain a complete Doppler-free profile of the hyperfine features. and then used the Moffat model to fit the results.

Our final results provide a good qualitative estimate and proof of concept for the saturation spectroscopy technique but for a more conclusive test of the accepted values an update of the current setup is required.

Acknowledgments

The author would like to thank Zachary Kluger for a laborious collaboration on performing the measurements and collecting the data, and also Dr. Eric Jones and Kristina Finnelli for their constant support and advising, and for equal partnership in the successful realization of this experiment, in particular in the tedious process of alignment and calibration of the experimental setup.

[1] Teach Spin Manual. *Instructors Manual*. 2002. Available online at: https://physics.indiana.edu/~courses/p451/background_info/TeachSpin_Manual_Optical_Pumping_of_Rubidium.pdf.

[2] Daniel A. Steck. *Rubidium 87 D Line Data*.2001. Unpublished, available online at: https://steck.us/alkalidata/rubidium87numbers.1.6.pdf.

[3] Department of Physics and Astronomy at Stony Brook University. *Diode Laser Saturation Spectroscopy of the D_2 Lines for rubidium Atoms*. Lab Manual, 2020.

[4] Wang J, Liu H, Yang G, Yang B, Wang J. Determination of the hyperfine structure constants of the Rb87 and Rb854D5/2state and the isotope hyperfine anomaly. Physical Review A 90, 2014.

[5] Ye J, Swartz S, Jungner P, Hall JL. Hyperfine structure and absolute frequency of the ^{87}Rb $5P_{3/2}$ state. Optics Letters 21: 1280, 1996.

[6] Preston DW. Dopplerfree saturated absorption: Laser spectroscopy. American Journal of Physics 64: 14321436, 1996.

[7] THORLABS SA210 Series Fabry-Pérot Interferometer. User guide. Available online at: https://www.thorlabs.com/thorproduct.cfm?partnumber=SA210-18C.

[8] THORLABS Laser Diode Controller. LDC200C Series Operation Manual. Available online at: https://www.thorlabs.com/thorproduct.cfm?partnumber=LDC205C.

[9] W. F. Smith, Experimental Physics: Principles and Practice for the Laboratory (CRC Press, Boca Raton, 2020).

[10] S. Bize, Y. Sortais, M. S. Santos, C. Mandache, A. Clairon, and C. Salomon, Europhysics Letters (EPL) 45, 558 (1999).